



The effect of the surface disordered layer on the photoreactivity of titania nanoparticles

J. Soria^a, J. Sanz^b, M.J. Torralvo^c, I. Sobrados^b, C. Garlisi^d, G. Palmisano^d, S. Çetinkaya^e, S. Yurdakal^e, V. Augugliaro^{f,*}

^a Instituto de Catálisis y Petroquímica, CSIC, C/Marie Curie 2, Cantoblanco, 28049 Madrid, Spain

^b Instituto de Ciencia de Materiales, CSIC, C/Sor Juana Inés de la Cruz, Cantoblanco, 28049 Madrid, Spain

^c Facultad de Ciencias Químicas, Universidad Complutense de Madrid, 28040 Madrid, Spain

^d Department of Chemical and Environmental Engineering, Masdar Institute of Science and Technology, PO BOX 54224, Abu Dhabi, United Arab Emirates

^e Kimya Bölümü, Fen-Edebiyat Fakültesi, Afyon Kocatepe Üniversitesi, Ahmet Necdet Sezer Kampüsü, 03200 Afyonkarahisar, Turkey

^f "Schiavello-Grillone" Photocatalysis Group, Dipartimento di Energia, Ingegneria dell'Informazione e Modelli Matematici (DEIM), Università degli Studi di Palermo, Viale delle Scienze (ed. 6), 90128 Palermo, Italy

ARTICLE INFO

Article history:

Received 6 February 2017

Received in revised form 15 March 2017

Accepted 16 March 2017

Available online 18 March 2017

Keywords:

TiO₂ acid treatment

Titania modifications

Disordered titania layer

Photocatalytic activity enhancement

4-Nitrophenol degradation

ABSTRACT

It is well known that the surface of metal oxide catalysts presents, usually, non-crystalline species containing impurities and low coordinated cations, which are observed in HRTEM images as a disordered layer of amorphous phase. Despite of being these species more accessible and less stable than the crystalline catalysts components, they have been rarely considered when analysing the catalyst activity. In this work, we have studied the effect of a treatment with HCl solution at pH = 0 on the characteristics of the disordered layer in two commercial anatase TiO₂ samples, using techniques such as TGA, ¹H MAS-NMR and HRTEM, and by determining these sample photocatalytic activity for the 4-nitrophenol degradation in aqueous suspension. The results indicate that associations of chlorine ions in amorphous titania chains and hydrated excess protons structures interact with anatase bridging hydroxyls. This interaction, that breaks Ti—O—Ti bonds between the anatase particles and the disordered layer species, enhances the anatase hydroxyls acidity, favouring the formation of O[−] radicals and eventually increasing the photocatalytic activity for 4-nitrophenol degradation under UV irradiation.

© 2017 Elsevier B.V. All rights reserved.

1. Introduction

Titanium dioxide is one of the most popular photocatalysts [1,2] due to its efficiency, chemical inertness, photostability, and ability to induce a great variety of redox reactions [3]. This semiconductor oxide is produced by various techniques in many of which titania is initially obtained as an amorphous or poorly crystalline solid so it needs a further thermal treatment to achieve the required properties. This treatment affects both the morphology and the structure of titania; the solid becomes denser and undergoes a phase

transition or more transitions from amorphous to anatase, rutile or brookite. Generally the phase transformation is not complete [4] so that the final solid contains crystals and a certain percentage of amorphous titanium dioxide with a very complicated structure [5–7]. In the majority of investigations the presence of amorphous phase is not taken into account with the consequence that all the catalysts features are exclusively attributed to the crystalline phases. Degussa P25 TiO₂, the most famous and tested photocatalyst, is generally reported to be composed only of anatase and rutile crystallites, whose ratio being typically in the 70:30–80:20 range. Ohtani et al. [8] reported that this catalyst contains also amorphous titania in a percentage varying from 2 to 13% and they conclude that P25 is a mixture of anatase (major), rutile and amorphous (minor) titania with different ratios depending not only on the sample production batch but also on position in a package.

The main consequence of the amorphous phase presence is that the majority of grain boundaries (and then most of the catalyst surface) is covered by a layer of disordered titania [9–12]; owing to the fact that photocatalytic processes involve the catalyst

* Corresponding author at: DEIM, University of Palermo, Viale delle Scienze, 90128 Palermo, Italy.

E-mail addresses: javiersoriaruiz@gmail.com (J. Soria), jsanz@icmm.csic.es (J. Sanz), torralvo@quim.ucm.es (M.J. Torralvo), isobrado@icmm.csic.es (I. Sobrados), cgarlisi1@masdar.ac.ae (C. Garlisi), gpalmisano@masdar.ac.ae (G. Palmisano), sidikacetinkayaa@gmail.com (S. Çetinkaya), sedatyurdakal@gmail.com (S. Yurdakal), vincenzo.augugliaro@unipa.it (V. Augugliaro).

surface, this layer, depending on its features, may affect in a considerable way the photocatalytic activity. It is commonly accepted that amorphous titania contains high concentrations of defects that will invariably function as rapid electron-hole recombination centres to render it inactive [13–15]. Specific investigations on the photocatalytic activity of amorphous TiO_2 are relatively few and their conclusions quite inconsistent. Amorphous titanium dioxide is reported to be an inefficient photocatalyst for H_2 production [16] and for 2-propanol oxidation and dehydrogenation [14]. Tanaka et al. [13], however, observed a negligible activity of amorphous TiO_2 for organic compounds degradation in comparison with commercial TiO_2 samples of different crystal forms and crystallinities. Significant photocatalytic rates for H_2 evolution [17] were obtained with hydrated samples of amorphous titania, this behaviour being observed also in amorphous and in hydrated forms of other metal oxides [18–21]. In a very recent paper devoted to establish a reliable method for the quantitative determination of the weight percent of amorphous titania, Lebedev et al. [22] found an inverse correlation between the photocatalytic activity and the amorphous phase content of different titania catalysts. The activity decreases by increasing the weight percentage of the amorphous phase; they also found that the partial removal of the amorphous phase by annealing or dissolution in acid solution leads to a significant activity increase.

The beneficial effect of an acid treatment on the photoactivity has been yet reported even if the reasons of this effect have not been deeply investigated. An acid treatment of TiO_2 electrode improves the photoelectric performance of dye-sensitized solar cells [23,24]; in particular the improvement is higher when the treatment is done by hydrochloric acid than by sulphuric, nitric, or phosphoric acid [25]. Degussa P25 TiO_2 , treated with HCl or H_2SO_4 solution and tested for Rhodamine B degradation under visible light [26], exhibited a significant enhancement of photoactivity, higher for HCl -treated sample than for the H_2SO_4 -treated one.

In order to obtain information on the effect of disordered titania layer on the photoactivity of anatase nanoparticles, in the present work we have studied, by XRD, adsorption-desorption measurements, TEM, HRTEM, TGA, DRS, Raman, DRIFT-IR, and ^1H MAS-NMR spectroscopies, the changes determined by an acid ($\text{pH} \sim 0$) treatment on the features of two commercial TiO_2 samples (Merck and BDH). These samples are composed by anatase crystals (major) and amorphous titania; the fact that these sample components exhibit different characteristics facilitates that the modifications induced by the acid treatment may be assigned to each of them. The effect of the acid treatment on the photoreactivity has been investigated by carrying out degradation runs of 4-nitrophenol (4-NP) in aqueous suspensions and determining the oxidation rates in the presence of untreated and treated TiO_2 samples. Previous studies on the 4-NP photocatalytic degradation in water in the presence of TiO_2 have shown that this process mainly yields carbon dioxide and very small amounts of *p*-benzoquinone and hydroquinone [27,28].

The main result of this investigation is that it proposes a likely explanation of the reasons why an HCl treatment modifies the structural, textural and photoactivity characteristics of amorphous-crystalline titania. The modifications induced by the acid treatment are of great concern as they may occur in all photocatalysts where amorphous and crystalline phases coexist.

2. Materials and methods

2.1. Samples treatment and characterization

BDH and Merck TiO_2 were used as received from the factory. The acid treatment was performed by suspending the samples (2.0 g of BDH or Merck TiO_2) in a balloon containing 1 M HCl aqueous

solution (500 mL). The balloon, fitted with a Graham condenser, was kept at 373 K for 8 h; after that the suspension was waited 16 h at room temperature (RT). The catalyst was separated by decantation and dialysed several times with deionised water until a neutral pH was reached. Then the catalyst was dried at 333 K by means of a rotary evaporator machine (Heidolph model M) working at 100 rpm; hereafter these samples are named as BDH_{ac} and Merck_{ac} . Aliquots of these samples were treated at RT for 14 h under vacuum (30 Torr) before performing XRD, TGA, Raman, UV-vis and DRIFT-IR investigations.

X-Ray diffraction analysis was performed by using XRD Bruker D8 Advance diffractometer with $\text{CuK}\alpha$ radiation of 1.54 Å, scan step size 0.0167° and a 2θ scan range of 10–80°. In order to check the presence of amorphous titania in the samples, the procedure reported by Jensen et al. [29] was followed. XRD diffractograms were recorded for mixtures of TiO_2 and CaF_2 (50%, w/w) and areas of 100% peaks of anatase (101) and CaF_2 (220) were determined. By comparing the ratio between the areas of those peaks to the ratios obtained by using the pure phases (1.25 for anatase), the relative amount of crystalline and amorphous phases was deduced.

Transmission electron microscopy (TEM) photographs were obtained with a JEOL JEM 2000FX microscope (operating at 200 kV) and a JEOL 3000 High-Resolution TEM microscope (operating at 300 kV). In each case, the sample was suspended in butanol and a drop of the suspension was deposited over a copper grid coated with a holey carbon support film. The time spent in analyzing different parts of samples was minimized to avoid degradation of particles surface. The TEM photographs were also used to determine the thickness of surface disordered layer as a function of nanoparticles size and so to get information on the effect of acid treatment on those layers. To this aim two groups of 150 particles were analysed for each sample by measuring the crystal size and the disordered layer thickness; even if the number of analysed particles is not high, the obtained distributions were almost the same.

TGA analyses were performed by using Netzsch STA 449 F3 thermal analysis equipment, in nitrogen flow. Samples of ca. 65 mg were used and the following temperature ramp was applied: temperature was increased from 303 K to 393 K at a rate of 5 K/min and the sample is kept at 393 K for 15 min; afterwards, temperature was increased from 393 K to 1023 K at a rate of 10 K/min. The temperature was finally decreased from 1023 K back to 303 K at a rate of 50 K/min. Adsorption-desorption measurements were performed in ASAP 2020 Micromeritics equipment. Prior to the adsorption experiments, the sample was out-gassed at 383 K for 3 h. For specific surface area calculations the value of 0.162 nm² has been used for the area occupied by a nitrogen molecule in a monolayer on flat surface [30]. The pore size distribution was obtained by the BJH method [31] using the Kelvin equation with the assumption of cylindrical pores [32].

The characteristic molecular vibrations of the surface groups of the powders were investigated by DRIFT-IR using Bruker VERTEX 80/80v, equipped with liquid nitrogen cooled MCT detector. The spectra were obtained in absorbance mode. For each spectrum, 512 consecutive scans at 4 cm⁻¹ resolution were acquired in 4000–400 cm⁻¹ wavenumber range. The UV-vis absorption spectra were obtained in air at RT in the wavelength range 300–600 nm using 2200 UV-vis Shimadzu spectrophotometer with BaSO_4 as the reference material; care was taken in order to record spectra with the same baseline. Raman spectroscopy was carried out by Witec Alpha 300R equipment, with an excitation wavelength of 532 nm and a laser power of ca. 75 mW. Scans were taken over an extended range (100–800 cm⁻¹) with 1 s integration time and 200 accumulations.

^1H magic angle spinning (MAS) NMR spectra were recorded after $\pi/2$ radiofrequency pulse irradiations at 400.13 MHz in AVANCE 400 (Bruker) spectrometer ($B_0 = 9.4$ T). In MAS-NMR experiments,

Table 1

Specific surface area and first order kinetic constant values for 4-NP degradation.

Catalyst	Specific surface area [m ² /g]	Kinetic constant [m/h]
BDH	10.5	2.41×10^{-4}
BDH _{ac}	10.3	4.60×10^{-4}
Merck	10.6	2.86×10^{-4}
Merck _{ac}	10.4	4.14×10^{-4}

samples were spun at 10 kHz around an axis inclined 54°44' with respect to the magnetic field. The number of scans was 100 and the time between successive experiments 5 s. The samples were investigated as received from the factory; a conventional vacuum line (residual pressure: 10⁻⁶ Torr) was used to evacuate them. To preserve desorption conditions, rotors were filled under nitrogen atmosphere inside a globe box. Spectra deconvolution was carried out with the Winfit (Bruker) software package. NMR chemical shift values were referred to those of tetramethyl-silane (TMS) signal, and lines intensity to that of the rotor cap used.

2.2. Photocatalytic set-up and procedure

A continuously stirred cylindrical beaker (volume: 250 mL; diameter: 6.7 cm) containing 150 mL of aqueous suspension was used as photoreactor. The suspension was irradiated by four fluorescent lamps (Philips, 8 W) with almost monochromatic emission at 365 nm. These lamps were positioned at a distance of 6.8 cm from the top of the suspension. The average value of the radiation energy impinging on the suspension was 2.1 mW cm⁻² and it was measured in the 315–400 nm range by a radiometer (Delta Ohm, DO 9721).

The photoreactivity runs were carried out at RT; the initial substrate concentration was 0.144 mM and the catalyst amount was 0.20 g L⁻¹. With such amount of BDH and Merck catalysts the suspension transmitted ca. 20% of the incident radiation so that all the catalysts particles were active for the photoreaction occurrence. The solution was adjusted to pH = 4 by adding HCl. Before switching on the lamps, the suspension was stirred for 30 min at RT in order to reach the thermodynamic equilibrium. The starting time of irradiation was taken as the zero time of the photocatalytic run. The contact of the suspension with the atmosphere guaranteed that the aqueous solution was saturated by oxygen during the course of the runs. The 4-NP adsorption under dark conditions was always quite low, i.e. ca. 3%. During the runs samples of reacting suspension were withdrawn at fixed time intervals; they were immediately filtered through a 0.45 µm hydrophilic membrane (HA, Millipore) before being analyzed.

Quantitative determination of 4-NP concentration was carried out by measuring the solution absorbance at the wavelength of 318 nm by means of 2200 UV-vis Shimadzu spectrophotometer; a multipoint calibration was preliminarily performed. The substrate mineralization extent was monitored by total organic carbon (TOC) determination carried out by 5000A Shimadzu analyzer. All used chemicals were provided by Sigma-Aldrich with a purity >99.0%.

3. Results and discussion

3.1. Morphology characteristics

The specific surface area values, determined by the adsorption-desorption measurements, are reported in Table 1; in the limit of experimental error, it seems that the acid treatment determines a small decrease of catalysts surface areas. The XRD patterns of all samples, both untreated and treated ones, indicate the presence of anatase (major) and brookite (traces) being the main peaks at $2\theta = 25.5^\circ, 38.0^\circ, 48.0^\circ, 54.5^\circ$ those characteristic of anatase TiO₂.

The XRD analysis clearly shows that the acid treatment does not modify the samples patterns, Fig. 1 of Supplementary Material (SM). The crystallinity absolute values, determined by following the Jensen et al. [29] procedure, were 65.9 and 63.9% for BDH and Merck samples, respectively, thus indicating that in these sample two components coexist: the anatase crystals and the amorphous titania. Merck sample contains a little more amount of amorphous titania than the BDH one. Those values did not change after the acid treatment thus indicating that at the treatment soft conditions, as expected, anatase does not dissolve and amorphous titania does not crystallize. It is important to outline that in this investigation the crystallinity values are not important *per se*; they only gave information on the presence of amorphous phases in the commercial samples and on their variation, if any, as a consequence of the acid treatment.

The TEM micrographs of the samples show aggregates of soldered smooth-surface anatase nanoparticles with polygonal boundaries and non-homogeneous crystal size, Figs. 1 and 2. These images show that the aggregates of the untreated and acidified Merck sample are less dense, presenting more holes, than those of the BDH ones. These images also show that the untreated sample aggregates present fewer holes than those of the acid treated ones, showing that the acid treatment diminishes the aggregates density. In fact, very small aggregates of 3–10 particles are frequently observed in the images of the BDH_{ac} and Merck_{ac} samples. The decrease of the aggregates density in the acid treated samples favors their nanoparticles disaggregation when dried samples are put in water. This effect, not observed for the untreated samples, indicates that the acid treatment has weakened the particles bonding. The crystals size distribution is similar in BDH and Merck samples, their mean values being 90 and 110 nm, respectively, Fig. 3.

The HRTEM images of the untreated and acid treated BDH and Merck samples show anatase nanoparticles covered by very thin (less than 3 nm) layers, formed by disordered titania species, Fig. 4; these species have been described as an assembly of very short (less than 1.5 nm) staggered chains of Ti–O octahedra [5]. These chains, constituted by very few titania octahedra, appear forming worm-like features, characteristic of amorphous titania, particularly at the boundaries of connected anatase nanoparticles. The distribution of this non-homogeneous layer thickness is reported in Figs. 5 and 6. These Figures show that the distribution of this layer thickness is broader for the untreated Merck sample than for the BDH one (0.7–2.5 and 0.7–1.5 nm respectively, with maximum value of 1.1 nm), indicating that the disordered titania species are more dispersed and/or more weakly bound to the anatase particles surface in the Merck sample than in the BDH one. Those Figures also show that the acid treatment increased the thickness of both samples disordered layer, presenting its maximum of 1.9 and 1.4 nm for the Merck_{ac} and BDH_{ac} sample, respectively. However, while the thickness distribution increased for the BDH_{ac} sample (0.7–2.0 nm), it decreased for the Merck_{ac} one (1.5–2.2 nm), by the disappearance of the thickest layers (more than 2.1 nm). The broadening of the disordered layer indicates that the acid treatment enhances the dispersion of the layer amorphous titania chains and/or it weakens the anatase-disordered layer interactions. These effects should result from the breaking of Ti–O–Ti bonds among the chains and between chains and anatase particles; the disappearance of the Merck thickest layers should suggest that some layers are detached from the anatase particles. The more compact distribution of the BDH_{ac} sample disordered layer thickness and the weaker effect of the acid treatment on the layer thickness in the BDH anatase particles boundaries than in those of the Merck sample, observed in the HRTEM images of Fig. 4, indicate that in the BDH sample the chains are more strongly condensed, inducing a more dense character of its anatase nanoparticles aggregates.

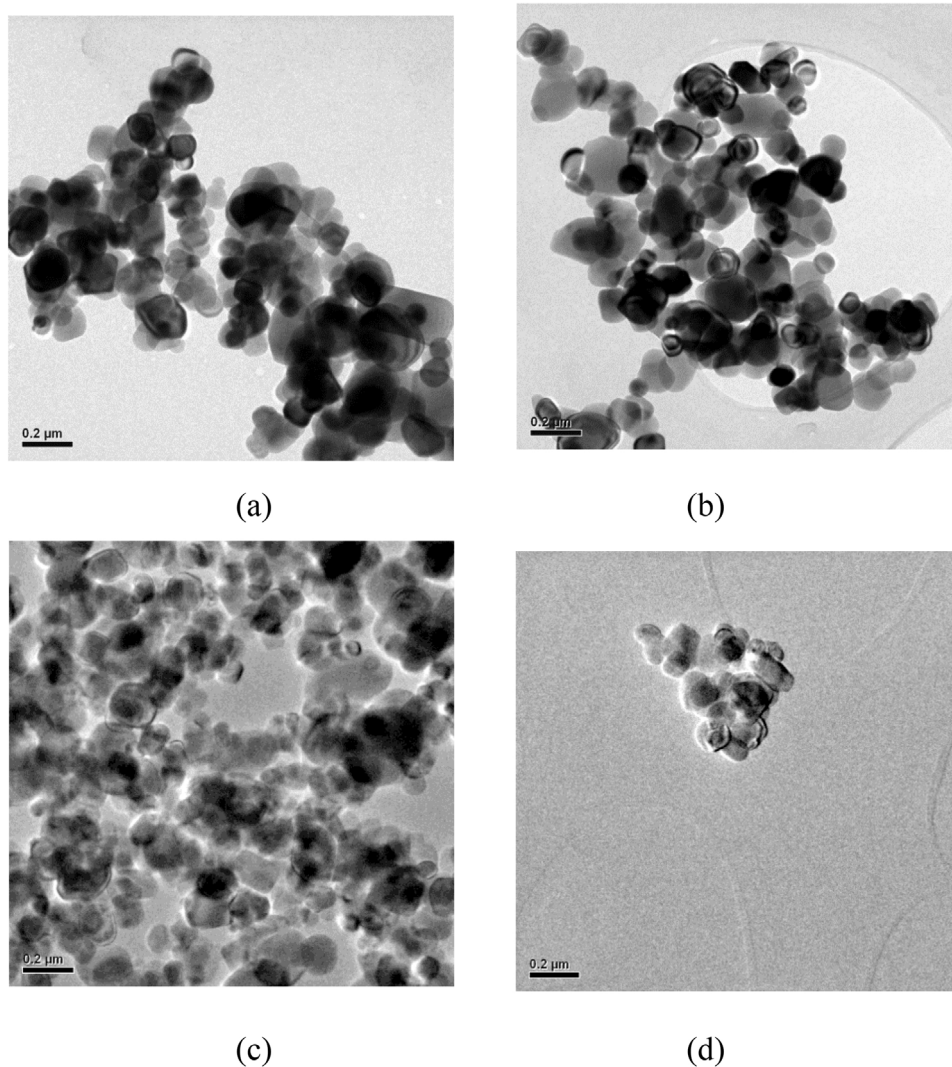


Fig. 1. TEM photographs of aggregates of BDH (a), BHD_{ac} (b), Merck (c), and Merck_{ac} (d) samples.

At this point, it is worthy to note that non-polar materials have a notable tendency to self-aggregate in polar solvents such as water, a phase separation phenomenon denoted as “hydrophobic effect” [33]. This effect can justify that the anatase particles of the acid treated aggregates, covered by hydrophobic amorphous titania chains, remain self-assembled in the acid solution but dispersed in pure water. However, to explain why in the present case the hydrophobic amorphous titania chains of the disordered layers are being dispersed, it is necessary to consider the particular characteristics of the water solution during the samples acid treatment. Considering that HCl molecules are decomposed in very acid aqueous solutions [34] with the formation of Cl[−] ions and protons, that should form hydrated excess proton structures, the interaction of these ions can lead to the generation of associated hydrophobe-hydrated proton structures of the type proposed by Agmon [35]. The formation of these associations is favored because the hydrated excess proton orients its lone electron pair toward the hydrophobic species, due to the amphiphilic character of the former [36,37]. When the samples are dried, some Cl[−] ions should be incorporated by ion exchange to the titania samples, preferentially to their amorphous titania species where the low coordination of some of their Ti cations [6] should favor that process. In this respect, a TPD study of chlorinated samples has shown simultaneous water and chlorine desorption peaks with maxima at about 420 and 700 K [38].

The chlorine-hydrated excess proton associations can act as a surfactant [37], impeding the occurrence of the strong hydrophobic phase separation in concentrated acid solutions. These associations, however, can play different roles depending on the Cl[−] ions location. When the Cl[−] ions are located in the interface between the anatase nanoparticles and the disordered layer, they can favor the breaking of the Ti—O—Ti bonds so facilitating the nanoparticles self-assembling. This effect should favor the anatase particles dispersion. On the other hand, if the Cl[−] ions are located in condensed amorphous titania chains of the disordered layer, the Ti—O—Ti bond breaking effect can induce a self-assembled nanostructuration of the chains [39]. This chains nanostructuration can explain the formation of worm-like features observed in the HRTEM images of the disordered layer, characteristic of amorphous titania species [5], Fig. 4d. So, the Cl[−] ions incorporation to the amorphous titania chains should enhance those species hydrophobic character and the stability of the associations of hydrophobe-hydrated proton structures beyond that of the hydronium ions [40].

3.2. Textural properties

The nitrogen adsorption-desorption isotherms of the untreated and acid treated samples are of type IV with a type H1 hysteresis loop at high relative pressures ($P/P_0 \sim 0.9$), Fig. 2SM. The pore

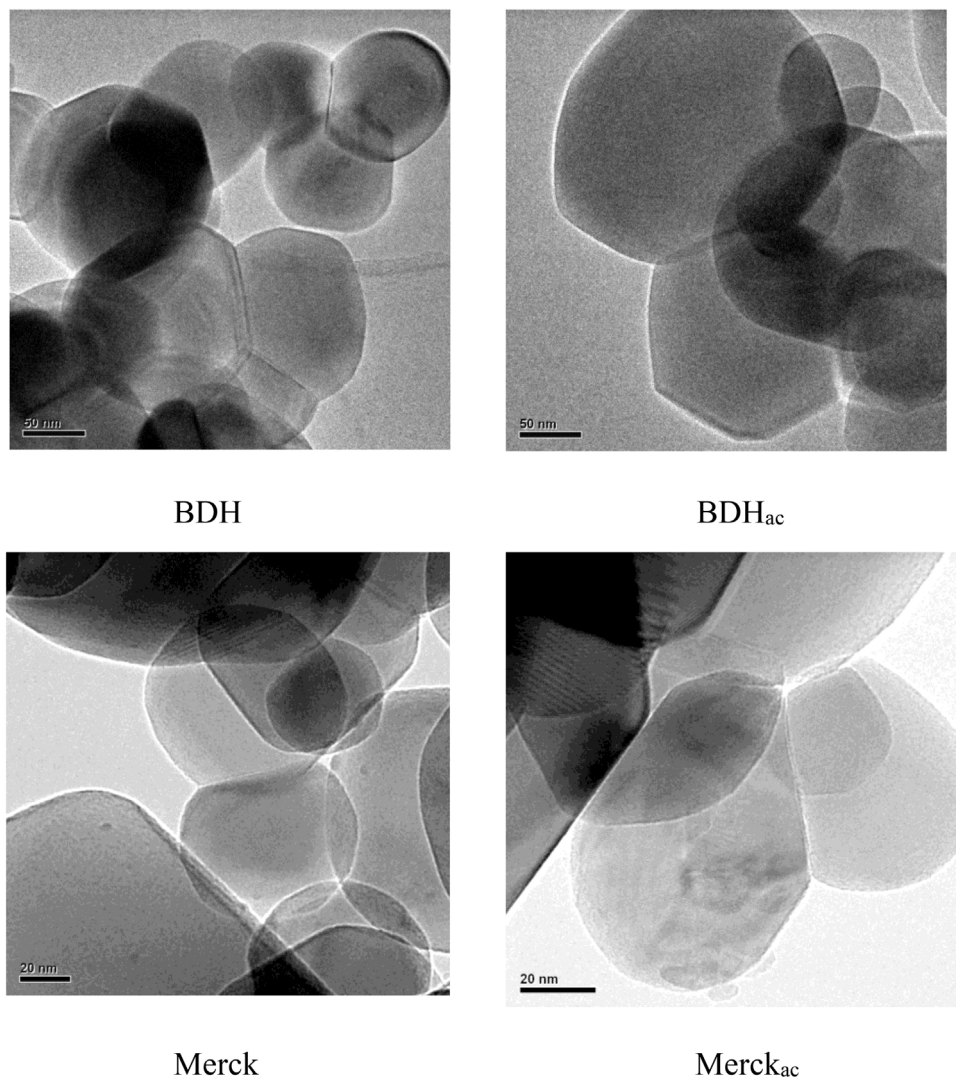


Fig. 2. TEM photographs of soldered particles with polygonal boundaries.

volume value is, in all cases, lower than $0.1 \text{ cm}^3/\text{g}$, Fig. 3SM. The acid treatment determines a measurable increase of the pore volume for both samples, more marked for the Merck_{ac} sample than for the BDH_{ac} one (19 and 10%, respectively). This increase indicates that the titania layer gets less dense and more disordered after the acid treatment. The pore width distributions for untreated and acidified BDH and Merck samples are reported in Fig. 3SM. They show that the acid treatment reduces the abundance of the pores with width of about 2 nm, more markedly in the Merck_{ac} than in the BDH_{ac} sample, while the biggest pores content increases, also more in the Merck_{ac} sample. These modifications indicate that the elimination of small pores, originated by amorphous titania chains in the anatase particles boundaries, induces the broadening of the biggest pores formed by those adjacent anatase nanoparticles. This feature could justify the decrease of surface area observed in both samples after the acid treatment, Table 1.

3.3. Thermogravimetric study

The thermogravimetric (TG) analysis of the untreated and acidified BDH and Merck samples shows that, though the greatest weight loss is only about 1.1%, the acid treatment produced clear effects by modifying the features of samples surface, Fig. 7. The untreated samples present similar TG profiles, showing a fast

weight loss at up to 395 K of 0.18 and 0.24%, respectively, followed by slow weight modifications at up to 1050 K (a small weight loss of 0.04% at up to 540 K and a small weight gain of 0.08% at up to 1050 K). Similarly, the profiles of BDH_{ac} and Merck_{ac} samples show a fast weight loss at up to 395 K, more marked than that of the untreated samples and composed of two components (one up to 385 K, of 0.28% and 0.36%, and the sharpest one of 0.23% and 0.15% in the 385–395 K range, respectively), and a slow weight loss more marked and extended than that presented by the untreated samples profiles (of about 0.55% up to 1043 K). So, the relatively similar shape of these four profiles, mainly formed by a fast and a slow weight losses at below and above 395 K respectively, seems to indicate that they are originated by the desorption of the same type of species. By considering that Li et al. [38] reported thermal desorption profiles of chlorinated anatase photocatalysts showing the simultaneous water and HCl desorption by heating up to about 873 K, the fast weight loss observed in the four profiles can be attributed to the desorption of weakly adsorbed water, together with some Cl^- ions desorbed as HCl molecules. On the other hand, the slow weight loss should be originated by desorption of chlorine-hydrated excess proton associations. The excess proton charge defect delocalization at the associations enhances the surface stabilization of the hydrated proton structures over the classical hydronium limit [40]. So, the acid treatment induces the

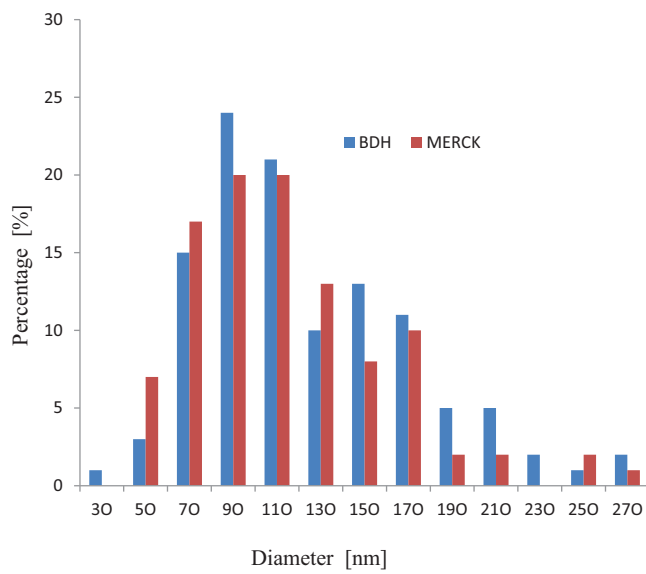


Fig. 3. Crystals size distribution of Merck and BDH samples.

increase of the fast and slow weight losses by favoring water H-bonding to those associations and the Cl^- ions incorporation to the amorphous titania chains, respectively.

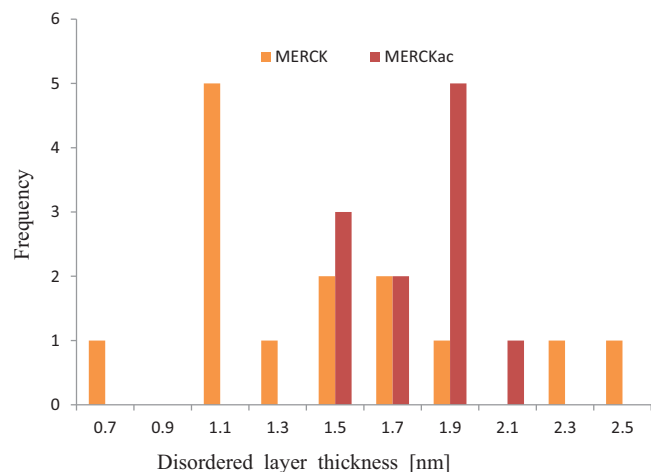


Fig. 5. Disordered layer distribution in Merck and Merck_{ac} samples.

As to concern the weight gain observed in the untreated samples, it can be produced by adsorption of oxygen molecules present as impurities in the nitrogen flow. It is likely that the commercial samples, owing to their preparation method, contain traces of Cl^- ions that are chemically bound to low coordinated Ti cations. At high enough temperature chlorine desorbs as HCl and in the

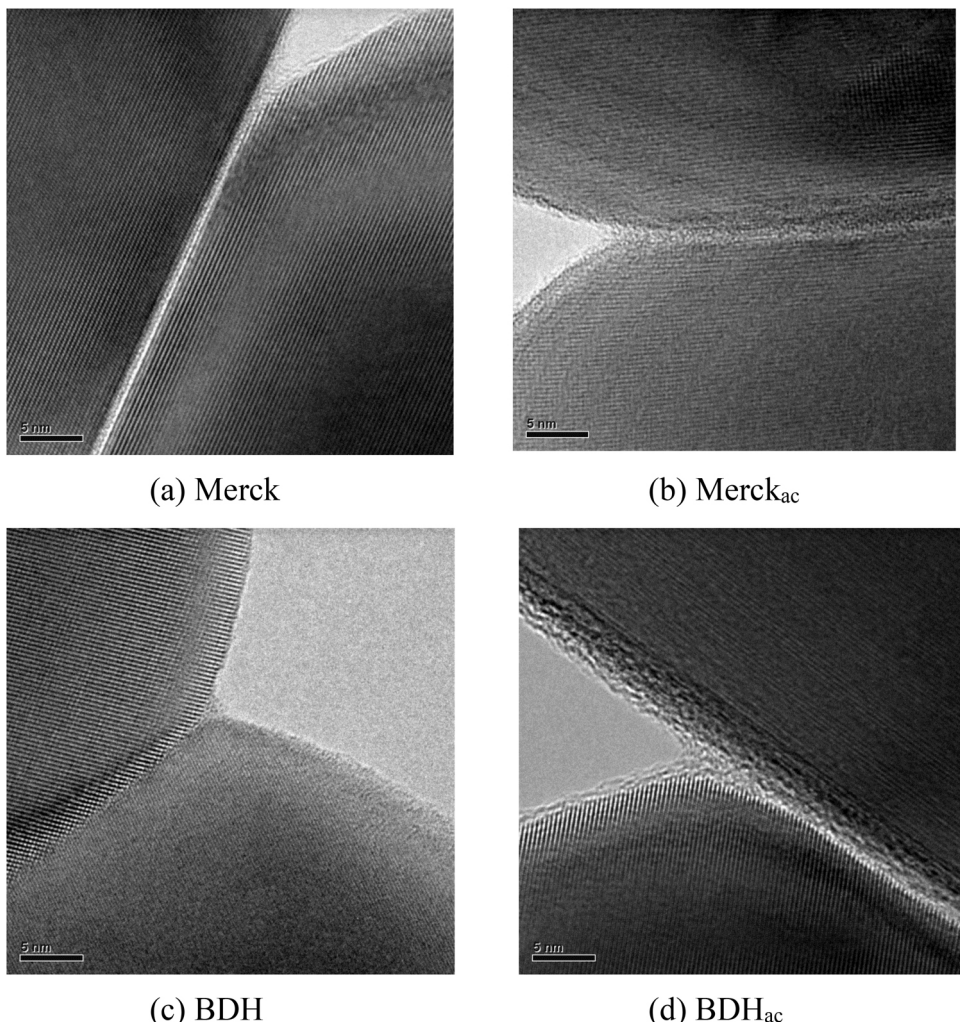


Fig. 4. HRTEM images of soldered crystals showing the effect of acid treatment.

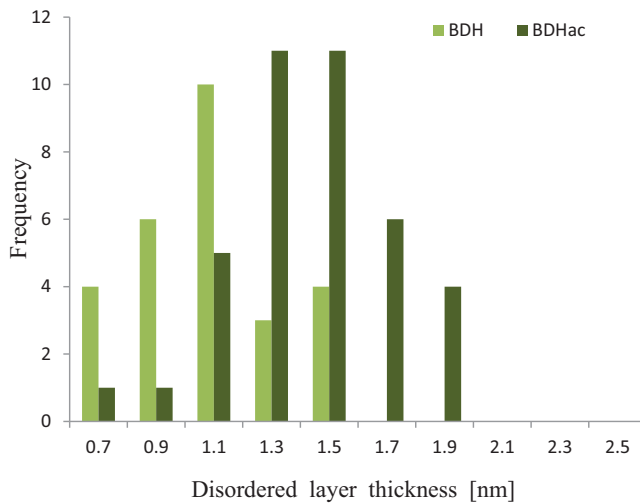


Fig. 6. Disordered layer distribution in BDH and BDH_{ac} samples.

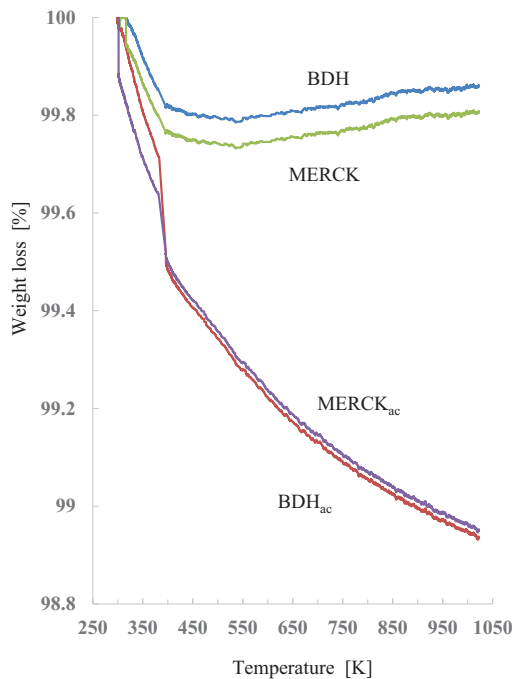


Fig. 7. Thermogravimetric profiles of untreated and acidified BDH and Merck samples outgassed at room temperature.

presence of oxygen the Ti cations should tend to adsorb oxygen molecules that, after their dissociation, should complete the octahedral coordination proper of Ti cations in TiO₂. So, the weight gain can be attributed to oxygen adsorption.

In order to check the effect of the heating temperature on the stability of the species originating the slowest weight loss, the TG profiles of Merck_{ac} and BDH_{ac} samples, heated under flowing nitrogen at 373 and 473 K, were recorded, Figs. 4SM and 5SM. These profiles show that the weight loss up to 800 K is 1.15 and 0.80%, respectively, for the BDH sample and 1.25 and 1.3% for the Merck one. Taking into account that the maximum weight loss by treating under flowing nitrogen at RT was about 1.1% for BDH_{ac} and Merck_{ac} samples, those values should indicate that heating under flowing nitrogen at 373 K enhances the Cl⁻ ions incorporation to the amorphous titania species of both samples. The treatment under flowing nitrogen at 473 K removes some of the Cl⁻ ions that had been incorporated to the BDH sample amorphous titania during the heating,

before reaching 473 K. The amount of retained water complexes depends on the number of Cl⁻ ions located at the samples surface; this number is particularly small in the BDH_{ac} sample.

3.4. Spectroscopic characterization of the disordered layer

3.4.1. Raman

Stoichiometric anatase crystals exhibit Raman modes at about 146 (E_g), 197 (E_g), 396 (B_{1g}), 515 (A_{1g}), and 639 (E_g) cm⁻¹ [41]. The anatase E_g scattering at 146 cm⁻¹ is of particular interest as it would shift in response to the amount of oxygen vacancies in the crystal lattice [42,43]. The Raman spectra of untreated BDH and Merck samples exhibit their E_g mode at 147.9 cm⁻¹, while the BDH_{ac} and Merck_{ac} samples show their E_g modes at 149.6 cm⁻¹, Fig. 6SM. The upwards shift of that E_g value from the 146 cm⁻¹ one corresponding to stoichiometric anatase can be due to the existence of oxygen vacancies in the anatase lattice [44] and/or to the amorphous titania present in the samples [45]. Considering that the percentage values of exposed {001} facets in anatase TiO₂, quantitatively obtained by measuring the intensity ratio of the E_g and A_{1g} peaks [46], are almost the same for Merck, Merck_{ac}, BDH, and BDH_{ac} samples (see those values in Table 1SM), it can be assumed that the crystalline phases are unaffected by the acid treatment. So, the upwards shift of the E_g value should be mainly due to the interaction of disordered titania with the anatase surface; during the acid treatment this interaction increases (as also the E_g shift) owing to the increase of the amorphous layer present on the anatase particles surface.

3.4.2. UV-vis

The UV-vis absorption spectra of untreated and acidified samples show that the acid treatment produces a small, but evident, shift of the samples absorption towards the visible region [38,47], Fig. 8. This shift is a clear clue that some chlorine ions have been incorporated to the catalyst surface. Adsorbed Cl⁻ ions have been reported to increase the catalysts surface acidity, which eventually enhances the photocatalytic activity [48].

3.4.3. DRIFT-IR

The DRIFT-IR spectra of the Merck, BDH, Merck_{ac} and BDH_{ac} samples treated with flowing nitrogen at RT are mainly formed by two very broad absorptions, in the range of 3800–2500 and 1800–400 cm⁻¹ and by some narrow lines at 3710, 1635, 1250, 1120, 920 and 710 cm⁻¹, Fig. 9. The similar shape of the high wavenumbers absorption, formed by overlapped broad bands, indicates that these bands correspond to the hydrated excess proton structures associated to Cl⁻ ions, forming the water complexes [35]. In this respect, it is worth noting that, in water-hydrophobic wall interfaces in strongly acid solutions, the hydrated excess proton is preferentially localized at the hydrophobe-water interfaces [40]. There, the water molecules around the hydronium ion are orientated, indicating a rigid hydrated proton structure. The excess proton charge defect delocalizes at the interfaces, being the Zundel-like form more probable than that of the Eigen-like one [40]. So, the broad shoulders at about 3380 and 2850 cm⁻¹ are characteristic of hydrated excess protons with Zundel-like and Eigen-like structure [35,49], respectively, while the shoulders at about 3250 and 3130 cm⁻¹ have been attributed to strongly H-bonded water [50,51]. The narrow bands at 1635 and 3715 cm⁻¹ should correspond to the complexes water bending mode and to the free OH stretching vibrations of water at those associations surface [52].

On the other hand two regions can be considered in the absorption at low wavenumbers, at 1900–1500 and 1500–400 cm⁻¹. The small absorption observed in the former should correspond to the bending mode of hydrated excess protons with Zundel-like structure (1880–1680 cm⁻¹) and Eigen one (1640–1580 cm⁻¹) [35,49], being overlapped by the narrow band at 1635 cm⁻¹. Meanwhile,

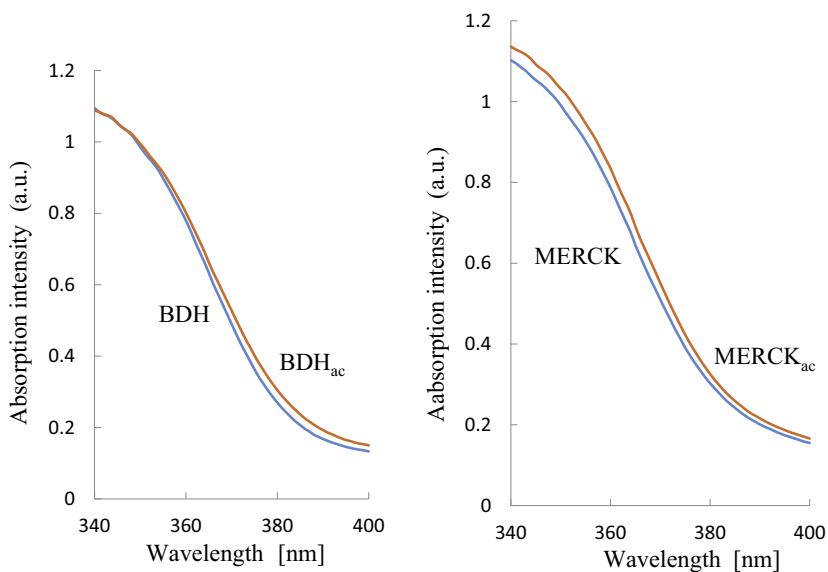


Fig. 8. UV-vis absorption spectra of untreated and acidified BDH and Merck samples.

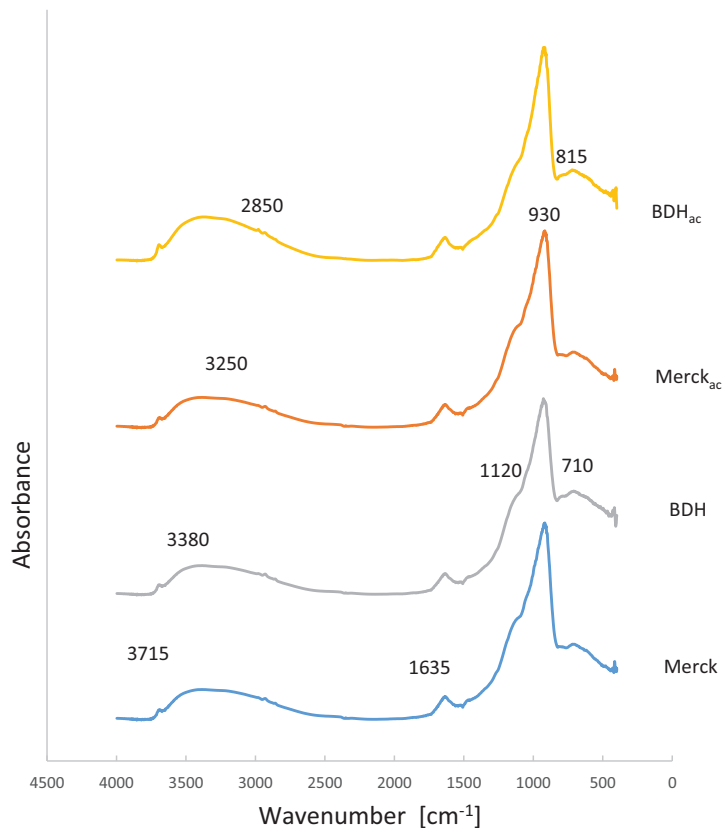


Fig. 9. DRIFT-IR spectra of untreated and acidified Merck and BDH TiO₂ recorded after outgassing at room temperature.

the 1500–400 cm⁻¹ spectra range appears formed by a broad absorption in the range of 1300–400 cm⁻¹, overlapped by several narrower bands at 1250, 1120, 930 and 710 cm⁻¹. Considering that the fundamental vibrations of TiO₂ nanocrystals, appearing as broad bands in the ranges of 550–653 cm⁻¹ and 436–495 cm⁻¹ and ascribed to the stretching vibrations of Ti–O and Ti–O–Ti bonds, respectively [52], are not resolved, the absorption in the spectral range of 700–1000 cm⁻¹ can be assigned to surface vibrations [53]. So, the 900–600 cm⁻¹ spectral range is characteristic of TiO₂ surface

phonon modes which denote the incomplete coordination of the surface layer ions [54]. Incorporation of water or other molecules to the coordination sphere of surface Ti cations leads to the deformation of the surface TiO₂ octahedrons. This deformation results in changes of the phonons spectra of the TiO₂ surface, namely in their shift towards higher frequencies. So, the strongest narrow bands at 930 and 1250 cm⁻¹ appear where the vibration modes of peroxide species, Ti–O–O–Ti, and hydroperoxide ones are usually observed [55]. These species might be formed on amorphous titania by O₂

reduction during the samples synthesis [56]. In addition, the bands centered at 1120 and 710 cm⁻¹ have been assigned to anatase Ti–OH vibrations [57] and to the stretching mode of its bridged Ti–O bonds [58], respectively. Meanwhile, the broad absorption can be attributed to lattice vibrations of condensed amorphous titania chains, because of its broader linewidth [59]. Being those chains located on the anatase surface, their vibration modes should contribute to the spectra more than those of anatase and should be more affected by impurities and adsorbed species.

The acid treatment produced similar effects on the spectra of both samples. The bands originated by the water complexes grew, suggesting the incorporation of Cl⁻ ions to the amorphous titania species, becoming adsorption sites of the water complexes. The narrow band at 3710 cm⁻¹ also shows a small increase. Meanwhile, the broad absorption originated by the lattice vibrations of condensed amorphous titania chains decreased, as result of the Cl⁻ ions incorporation to those species. The incorporation of Cl⁻ ions to amorphous titania chain, replacing lightly bound oxygen ones, generates strains in the chains due to the bigger Cl⁻ ions atomic radii than oxygen ions (1.81 Å) and O (1.32 Å) [48].

3.4.4. MAS-NMR

The ¹H MAS-NMR spectra of BDH and Merck samples are mainly formed by a broad band (line A) centered at 5.8 and 6.9 ppm, with a linewidth of 5 and 6 ppm, respectively, Figs. 10 A and 11 A. In hydrophilic anatase samples prepared by hydrolysis of titanium alkoxides (samples T and HT), a narrow line at 5.6 ppm was ascribed to adsorbed water, interacting with anatase OH groups [60,61]; in these samples proton exchange processes averaged chemical shift values of water and OH groups proton signals [62]. In commercial BDH and Merck samples studied here, line A was more shifted in the Merck than in BDH sample towards positive values, indicating that protons of OH groups display a higher acid character or maintain stronger hydrogen bonds. On the other hand, the line A of these two samples was much broader than that observed in highly hydrophilic T and HT samples. Considering that the line A width increases with decreasing mobile water, the broad line A detected in the BDH and Merck samples spectra indicates, in agreement with TG profiles, the presence of a small amount of water adsorbed in these samples.

The spectra deconvolution shows that line A is formed by two bands, one at 5.1 or 6.5 ppm and another at 6.5 or 7.5 ppm in BDH and Merck spectra, respectively. The chemical shift of BDH bands are very close to those observed for terminal and bridging hydroxyls of HT and T samples, where the amount of amorphous titania content was small [60]. Meanwhile, the chemical shifts of the bands at 6.5 and 7.5 ppm in the Merck sample are close to those of bands at 6.7 and 7.5–8.1 ppm observed in samples prepared by TiCl₄ hydrolysis, where a considerable amount of amorphous material was present [63]. From this fact, it is reasonable to conclude that the Merck sample has a higher amount of disordered material than the BDH one. On the other hand, chemical shift of line A in the BDH spectrum is similar to that in T or HT samples, where chlorine was absent, suggesting that the chlorine content of the BDH sample must be very low [60,61].

The deconvolution of ¹H MAS-NMR spectra also showed three weak lines at 10, 3 and 1 ppm, stronger in the Merck than in the BDH spectrum, contributing to the apparent line A broadening. Their chemical shifts appear significantly more separated from that of the mobile water than those of anatase hydroxyls protons. So, the line at 10 ppm and those at 3 and 1 ppm have been assigned to bridging and terminal hydroxyls of amorphous titania. The position of these bands indicates that OH groups of the amorphous phase display a bigger acid and basic character than those of the anatase samples. The line at 1 ppm could correspond to OH groups bonded

to Ti cations with coordination number lower than six [63] or to OH groups bonded to a lower amount of Ti cations in the amorphous phase. In the last case, OH groups should display a basic character. The resolution of lines ascribed to anatase and amorphous titania hydroxyls supports the absence of mobile water that averages chemical shift of OH bands.

In acid treated samples, ¹H MAS-NMR spectra display narrowed anatase components, shifted towards more positive values, and a new narrow intense component at 1 ppm previously ascribed to amorphous titania. The anatase band narrowing has been associated with the partial elimination of terminal hydroxyls during acid treatments. The shift of the bridging OH groups from 5.8 to 6.4 ppm and from 6.8 to 7.2 ppm has been ascribed to the acidity increase of those hydroxyls in treated samples, increase whose more likely origin is the Cl⁻ incorporation. The observed shifts could also be ascribed to formation of stronger hydrogen bonds of OH groups.

The retention of chlorine species enhances the hydrophobic character of the amorphous titania chains, facilitating the association of Cl⁻ ions and hydrated excess proton with Zundel-like structure [35]. The asymmetric behavior of the hydronium ion structure, resulting from its charge distribution, makes one end strongly hydrophobic while the other one is even more hydrophilic than water molecules. These species amphiphilic character can facilitate their behavior like surfactants [36] that stick to Cl⁻ ions of hydrophobic amorphous titania chains with their hydrophobic side by proton exchange and to anatase bridging hydroxyls with the hydrophilic one. This interaction should enhance hydroxyls acidity [48,64], originating the line A shift to more positive values. The increase of catalysts acidity is a known effect of chlorine incorporation [65,66]; however, the samples heating should favor the elimination of retained HCl species.

The increment of the narrow line at about 1 ppm, more marked in the Merck_{ac} spectrum than in the BDH_{ac} one, Figs. 10 B and 11 B, has been ascribed to a modification of the amorphous phase interacting with anatase particles surface. This modification is a consequence of the acid treatment, affecting the chains bonding to anatase particles and to other chains, as illustrated by HRTEM images. The incorporated ions should weaken interactions of amorphous titania chains with other chains and with anatase particles. This effect can lead to the Ti–O–Ti breaking, shortening the chains size and increasing the chains mobility with the eventual elimination of the chain association to anatase particles surface. The incorporation of Cl⁻ ions to the amorphous chains could also decrease the Ti cations coordination number, favoring the formation of terminal OH group, stable under strongly acid conditions in those cations coordination sphere. All these facts support the detection of the narrow line at 1 ppm in ¹H MAS-NMR spectra of acid treated samples. In agreement with previous information, this line at 1 ppm is more intense in the Merck_{ac} sample, where the amount of amorphous phase is higher. The chlorine ions incorporation originates the decrease of the amorphous titania surface vibrations (broad band at 1300–400 cm⁻¹ in DRIFT-IR spectra), stronger in the Merck_{ac} spectrum than in the BDH_{ac} one.

Previous studies on HP samples with increasing durations of thermal treatment [63] have shown that, while the condensation degree of their amorphous titania chains on anatase particles was growing, the narrow line at about 1 ppm was growing very slowly in NMR spectra. This behavior indicated that this line was not originated by OH groups bound to four fold coordinated Ti cations, the coordination of the Ti cations in TiCl₄ molecules. This result and the near absence of the line at 1 ppm in the NMR spectra of untreated samples indicate that this line could be originated by protons of OH groups bonded to five fold coordinated Ti cations of the amorphous chains. This coordination number is the most abundant in the Ti cations of amorphous titania [7]. The increased hydrophobic character and mobility of the chlorinated chains favor the condensation

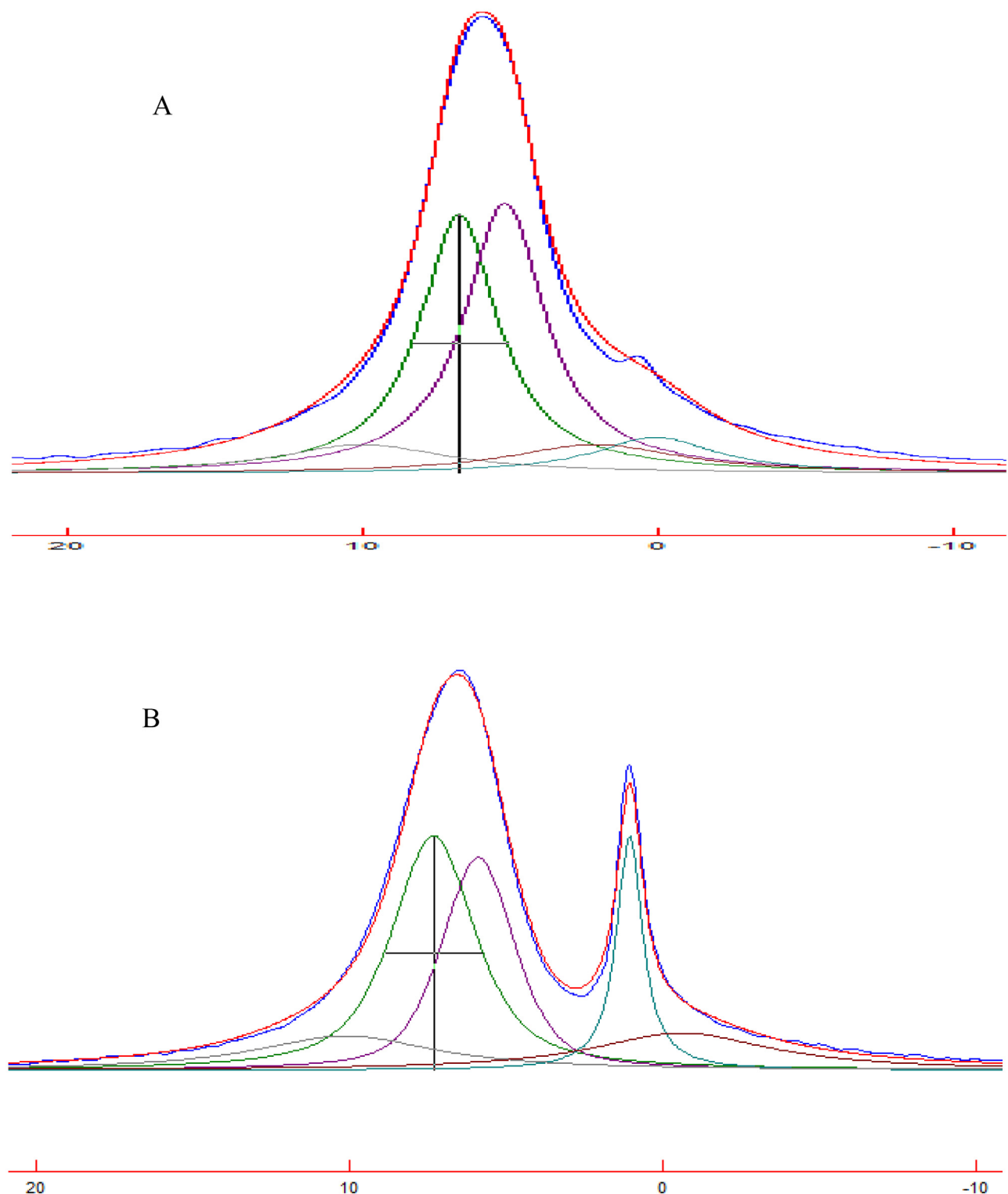


Fig. 10. ^1H MAS NMR spectra of the BDH TiO_2 before and after acid treatment.

and nanostructuration of some of them, by the hydrophobic effect, forming the worm-like features observed by HRTEM images. This chains redistribution can also originate the nanopores with size lower than 2 nm, observed in the samples pore size distribution curve. The stronger increase of the band at 1 ppm in the Merck_{ac} spectrum than in the BDH_{ac} one indicates that more amorphous titania chains have been nanostructured in the Merck_{ac} than in the BDH_{ac} sample. In both BDH and Merck samples acid treatment produces an increase of OH groups acidity but the amount of water

stabilized on the anatase surface does not increase in an important way.

3.5. Photoreactivity

Preliminary runs showed that in the absence of either light or oxygen no reactions take place. The 4-NP oxidation only produced carbon dioxide and small amounts of *p*-benzoquinone and hydroquinone. In the course of the runs the concentrations of 4-NP and

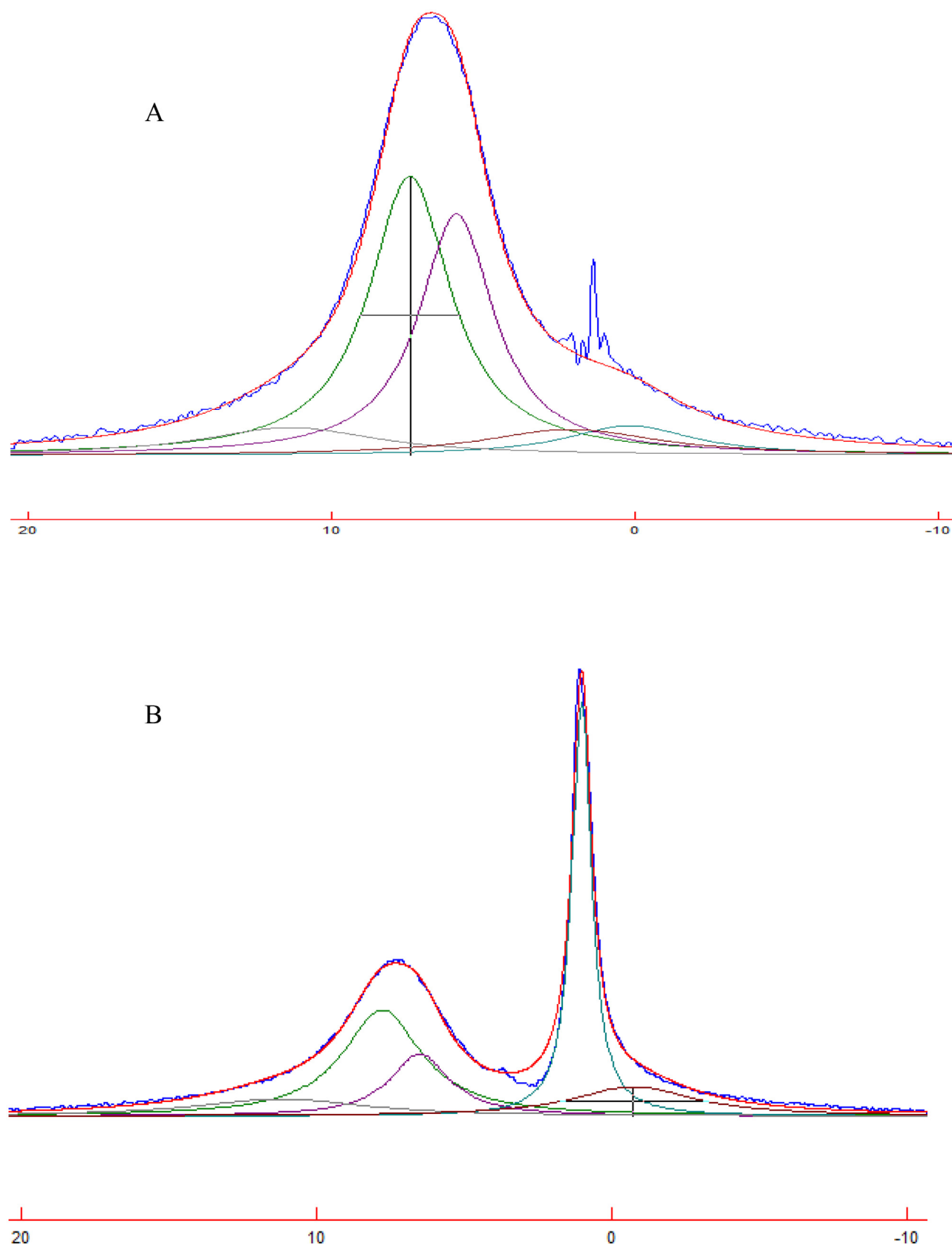


Fig. 11. ^1H MAS NMR spectra of the Merck TiO_2 before and after acid treatment.

total organic carbon (TOC) were measured. The CO_2 produced in the reactor was extrapolated from the TOC values as no organic volatile species are formed during the reaction [27,28].

For all the degradation runs the 4-NP concentrations showed an exponential dependence on irradiation time indicating a first order kinetic law for surface reaction. By considering that the 4-NP

concentration, $C_{4\text{-NP}}$, is the parameter experimentally measured, the 4-NP degradation rate, $-r_{4\text{-NP}}$, may be written in terms of Langmuir-Hinshelwood model as:

$$(-r_{4\text{-NP}}) \equiv -\frac{1}{S} \frac{dN_{4\text{-NP}}}{dt} = -\frac{V}{S} \frac{dC_{4\text{-NP}}}{dt} = k_{\text{Ox}} \theta_{4\text{-NP}} \\ = k_{\text{Ox}} \frac{K_{4\text{-NP}} C_{4\text{-NP}}}{1 + K_{4\text{-NP}} C_{4\text{-NP}}} \approx k_{\text{Ox}} K_{4\text{-NP}} C_{4\text{-NP}} = k C_{4\text{-NP}} \quad (1)$$

in which S is the surface area of catalyst present in the photoreactor, V the reaction volume, k_{Ox} the rate constant for 4-NP oxidation, $\theta_{4\text{-NP}}$ the fractional sites coverage by 4-NP molecules and $K_{4\text{-NP}}$ the 4-NP equilibrium adsorption constant. In Eq. (1) the assumption is done that the 4-NP concentration is low so that the following inequality holds: $1 \gg K_{4\text{-NP}} C_{4\text{-NP}}$ and then the reaction kinetics gets first order.

By fitting the integrated equation of Eq. (1) to the experimental data, the values of k have been obtained. Table 1 reports the values of this constant. It must be noted that the kinetic constant values are normalized with respect to the catalyst surface area, so that they can be used for comparing the specific surface reactivity.

The higher value of the 4-NP oxidation constant for Merck sample than for the BDH one, when both of them show almost the same crystal size and crystallinity, could be considered an unexpected result. However, this apparent discrepancy can be explained considering the different characteristics of the amorphous titania contained by these two samples. According to the ^1H MAS-NMR spectra, the disordered titania in the BDH sample is strongly condensed and mainly concentrated on the anatase particles boundaries, as shown by the little interaction of its hydroxyls with those of anatase particles. In these conditions the disordered titania layers which partially cover the BDH anatase crystals should act as recombination centres of photogenerated pairs. On the contrary, the disordered titania in the Merck sample is more weakly condensed and more dispersed on the titania surface, with its hydroxyls markedly affecting the anatase ones. Owing to these features, it is likely that part of titania layers covering anatase crystals is so thin that it behaves as a quasi-crystalline phase and so it is active for the photoreaction occurrence.

The acid treatment determines an evident increase of the photoreactivity: 1.9 times for BDH sample and 1.5 times for Merck one. Among the modifications determined by the acid treatment, those able to justify that increase are: (i) the redshift of radiation absorption; (ii) the decrease of the agglomerates size of the suspension; and (iii) the modification of disordered titania layer on the anatase surface. By considering that the redshift is quite low (Fig. 8) and that the used radiation source is almost monochromatic, it may be concluded that this effect may contribute to the photoreactivity increase but not justify the high observed one.

The decrease of agglomerate size certainly increases the radiation absorption by the suspension; however, the amount of BDH and Merck catalyst was chosen in order to transmit only the ca. 20% of the incident radiation. The same amount of powder with smaller aggregates could absorb all the incident radiation but in this case the photoreactivity increase should be of 25% in the best of cases, i.e. in low radiation intensity; so, as for the previous case, this effect could increase the photoreactivity but not justify that high increase.

Based on above considerations, the greatest responsibility of the photoreactivity increase for both samples can be attributed to the modification of the disordered titania layer present on the anatase crystals surface. It is important to note that, if the BDH and Merck samples were constituted only by anatase crystals, it should be very difficult to explain the effect of acid treatment on the photoreactivity increase. This increase should be originated by chlorine incorporation, mainly, into the samples amorphous component, which is the first effect of acid treating the samples, according their

characterization results. The interacting by H-bonding of anatase bridging hydroxyls with associations of incorporated chlorine and Zundel-like cation enhances those hydroxyls acid character. This improved hydroxyls acidity favors their deprotonation under UV irradiation and the trapping of photogenerated holes by the bridging O_2^- ions left, with the formation of O^- radicals [67] which can act as active species for 4-NP oxidation.

The higher increase of the BDH_{ac} sample photoactivity than that of the Merck_{ac} sample after the acid treatment (1.9 times for BDH_{ac} sample and 1.5 times for Merck_{ac} one) can be explained by the higher increase of the narrow line at about 1 ppm in the Merck_{ac} NMR spectrum than in the BDH_{ac} one. As the increase of that band is related to the amount of amorphous titania chains that have been restructured, the higher increase of that band indicates that less Cl^- ions are available for associations with hydrated excess protons, which justifies the lower increase of the photoactivity of the Merck_{ac} sample than of BDH_{ac} one. This effect is more important for BDH than for Merck sample owing to the fact that, as said before, the disordered titania in the BDH sample is more condensed and concentrated on the anatase particles boundaries and therefore it may be more strongly affected by the acid treatment.

4. Conclusions

The results indicate that the features of TiO_2 catalysts, constituted both by crystals and amorphous titania, are determined by both components. In fact a simple acid treatment is able to weaken the bonding of disordered titania to the anatase nanoparticles surface, determining a lesser condensation degree of amorphous titania, particularly important at the anatase particles surface. The disordered titania undergoes an important modification that may be ascribed to some depolymerization of Ti polyhedra, going from sixfold to a five or fourfold coordination.

The acid treatment not only affects the structural and textural characteristics of titania samples but also it induces a significant increase of the TiO_2 samples photoactivity [22]. This increase, observed in both Merck_{ac} and BDH_{ac} samples, should be due to the modification of the disordered titania layers on the anatase crystals. In fact the first effect of HCl treating the samples is the chlorine incorporation, mainly, into the samples amorphous component and the formation of Zundel-like structures with that chlorine. The interaction by H-bonding of anatase bridging hydroxyls with those structures enhances those hydroxyls acid character and eventually the photoactivity under UV irradiation. This effect is more important for BDH_{ac} than for Merck_{ac} sample; in fact, despite of their almost equal content of disordered titania, amorphous titania in the BDH sample is more condensed and concentrated than in the Merck one and then photoactivity can be more strongly affected by the acid treatment.

The reported study shows how a simple acid treatment can strongly affect structural and textural characteristics of the amorphous/disordered component present in titania samples, leaving the crystalline component nearly unaffected. These modifications are of great concern as they may occur in all the not completely crystalline solids which are currently used in thermal catalysis and all the different areas of photocatalysis.

Acknowledgments

Dr. Thomas Delclos at Masdar Institute of Science and Technology is gratefully acknowledged for technical support. Mrs. S. Martínez at ICMM (CSIC, Madrid) is gratefully acknowledged for technical support in NMR measurements.

This research did not receive any specific grant from funding agencies in the public, commercial, or not-for-profit sectors.

Appendix A. Supplementary data

Supplementary data associated with this article can be found, in the online version, at <http://dx.doi.org/10.1016/j.apcatb.2017.03.045>.

References

- V. Augugliaro, V. Loddo, M. Pagliaro, G. Palmisano, L. Palmisano, *Clean by Light Irradiation. Practical Applications of Supported TiO₂*, The Royal Society of Chemistry, Cambridge, 2010.
- A. Fujishima, T.N. Rao, D.A. Tryk, *Titanium dioxide photocatalysis*, J. Photochem. Photobiol. C: Photochem. Rev. 1 (2000) 1–21.
- A. Fujishima, K. Hashimoto, T. Watanabe, *Photocatalysis. Fundamentals and Applications*, BKC Inc., Tokyo, 1999.
- J. Sanz, J. Soria, I. Sobrados, S. Yurdakal, V. Augugliaro, Influence of amorphous TiO₂ on Titania nanoparticle growth and Anatase-to-Rutile transformation, J. Phys. Chem. C 116 (2012) 5110–5115.
- V. Petkov, G. Holzhüter, U. Tröge, Th. Gerber, B. Himmel, Atomic-scale structure of amorphous TiO₂ by electron, X-ray diffraction and reverse Monte Carlo simulations, J. Non Cryst. Solids 231 (1998) 17–30.
- H. Zhang, B. Chen, J.F. Banfield, G.A. Waychunas, Atomic structure of nanometer-sized amorphous TiO₂, Phys. Rev. B 78 (2008) 214106.
- K. Kaur, S. Prakash, N. Goyal, R. Singh, P. Entel, Structure factor of amorphous TiO₂ nanoparticle: molecular dynamics study, J. Non-Cryst. Solids 357 (2011) 3399–3404.
- B. Ohtani, O.O. Prieto-Mahaney, D. Li, R. Abe, What is Degussa (Evonik) P25? Crystalline composition analysis, reconstruction from isolated pure particles and photocatalytic activity test, J. Photochem. Photobiol. A: Chem. 216 (2010) 179–182.
- D.R. Clarke, Grain boundaries in polycrystalline ceramics, Ann. Rev. Mater. Sci. 17 (1987) 57–74.
- N. Kopidakis, N.R. Neale, K. Zhu, J. van de Lagemaat, A.J. Frank, Spatial location of transport-limiting traps in TiO₂ nanoparticle films in dye-sensitized solar cells, Appl. Phys. Lett. 87 (2005) 202106.
- P. Docampo, S. Guldin, U. Steiner, H.J. Snaith, Charge transport limitations in self-assembled TiO₂ photoanodes for dye-sensitized solar cells, J. Phys. Chem. Lett. 4 (2013) 698–703.
- K.P. McKenna, A.L. Shluger, Electron-trapping polycrystalline materials with negative electron affinity, Nat. Mater. 7 (2008) 859–862.
- K. Tanaka, M.F.V. Capule, T. Hisanaga, Effect of crystallinity of TiO₂ on its photocatalytic action, Chem. Phys. Lett. 187 (1991) 73–76.
- B. Ohtani, Y. Ogawa, S.I. Nishimoto, Photocatalytic activity of amorphous-anatase mixture of Titanium(IV) oxide particles suspended in aqueous solutions, J. Phys. Chem. B 101 (1997) 3746–3752.
- S.M. Waita, B.O. Aduda, J.M. Mwabora, C.G. Granqvist, S.E. Lindquist, G.A. Niklasson, A. Hafeldt, G. Boschloo, Electron transport and recombination in dye sensitized solar cells fabricated from obliquely sputter deposited and thermally annealed TiO₂ films, J. Electroanal. Chem. 605 (2007) 151–156.
- R.S. Davidson, C.L. Morrison, J. Abraham, A comparison of the photochemical reactivity of polycrystalline (anatase), amorphous and colloidal forms of titanium dioxide, J. Photochem. 24 (1984) 27–35.
- Z. Zhang, P.A. Maggard, Investigation of photocatalytically-active hydrated forms of amorphous titania, TiO₂·nH₂O, J. Photochem. Photobiol. A: Chem. 186 (2007) 8–13.
- H. Kominami, K. Oki, M. Kohno, S.I. Onoue, Y. Kera, B. Ohtani, Novel solvothermal synthesis of niobium(V) oxide powders and their photocatalytic activity in aqueous suspensions, J. Mater. Chem. 11 (2001) 604–609.
- C.Y. Wu, X.P. Zhao, Y.J. Ren, Y.H. Yue, W.M. Hua, Y. Cao, Y. Tang, Z. Gao, Gas-phase photo-oxidations of organic compounds over different forms of zirconia, J. Mol. Catal. A: Chem. 229 (2005) 233–239.
- A. Kudo, A. Tanaka, K. Domen, K. Maruya, K. Aika, T. Ohnishi, Photocatalytic decomposition of water over NiO-K₄Nb₆O₁₇ catalyst, J. Catal. 111 (1988) 67–76.
- T. Takata, K. Shinohara, A. Tanaka, M. Hara, J.N. Kondo, K. Domen, A highly active photocatalyst for overall water splitting with a hydrated layered perovskite structure, J. Photochem. Photobiol. 106 (1997) 45–49.
- V.A. Lebedev, D.A. Kozlov, I.V. Kolesnik, A.S. Poluboyarinov, A.E. Becerikli, W. Grünert, A.V. Garshev, The amorphous phase in titania and its influence on photocatalytic properties, Appl. Catal. B: Environ. 195 (2016) 39–47.
- D.W. Park, K.H. Park, J.W. Lee, K.J. Hwang, Y.K. Choi, Hydrochloric acid treatment of TiO₂ electrode for quasi-solid-state dye-sensitized solar cells, J. Nanosci. Nanotechnol. 7 (2007) 3722–3726.
- L. Song, P. Du, X. Shao, H. Cao, Q. Hui, J. Xiong, Effects of hydrochloric acid treatment of TiO₂ nanoparticles/nanofibers bilayer film on the photovoltaic properties of dye-sensitized solar cells, Mat. Res. Bull. 48 (2013) 978–982.
- S. Hao, J. Wu, L. Fan, Y. Huang, J. Lin, Y. Wei, The influence of acid treatment of TiO₂ porous film electrode on photoelectric performance of dye-sensitized solar cell, Sol. Energy 76 (2004) 745–750.
- S.-K. Park, H. Shin, Effect of HCl and H₂SO₄ treatment of TiO₂ powder on the photoinduced degradation of aqueous rhodamine B under visible light, J. Nanosci. Nanotechnol. 14 (2014) 8122–8128.
- A. Di Paola, V. Augugliaro, L. Palmisano, G. Pantaleo, E. Savinov, Heterogeneous photocatalytic degradation of nitrophenols, J. Photochem. Photobiol. A: Chem. 155 (2003) 207–214.
- S. Yurdakal, V. Loddo, G. Palmisano, V. Augugliaro, H. Berber, L. Palmisano, Photocatalytic degradation of 4-nitrophenol in a continuous reactor containing titanium dioxide supported on glass beads, J. Adv. Oxid. Technol. 11 (2008) 501–509.
- H. Jensen, K.D. Joensen, J.-E. Jørgensen, J.S. Pedersen, G. Søgaard, Characterization of nanosized partly crystalline photocatalysts, J. Nanopart. Res. 6 (2004) 519–526.
- F. Rouquerol, J. Rouquerol, K. Sing, *Adsorption by Powders and Porous Solids*, Academic Press, London, 1999.
- E.P. Barret, L.G. Joyner, P.P. Halenda, The determination of pore volume and area distributions in porous substances. I. Computations from nitrogen isotherms, J. Am. Chem. Soc. 73 (1951) 373–380.
- J.C. Broekhof, J.H. Deboer, Studies on pore systems in catalysts: XII. Pore distributions from the desorption branch of a nitrogen sorption isotherm in the case of cylindrical pores A. An analysis of the capillary evaporation process, J. Catal. 10 (1968) 368–376.
- C. Tanford, The hydrophobic effect and the organization of living matter, Science 200 (1978) 1012–1018.
- A. Vargas-Caamal, J.L. Cabellos, F. Ortiz-Chi, H.S. Rzepa, A. Restrepo, G. Merino, How many water molecules does it take to dissociate HCl? Chem.: Eur. J. 22 (2016) 2812–2818.
- N. Agmon, Structure of concentrated HCl solutions, J. Phys. Chem. A 102 (1998) 192–199.
- H. Chen, J. Xu, G.A. Voth, Unusual hydrophobic interactions in acidic aqueous solutions, J. Phys. Chem. B 113 (2009) 7291–7297.
- M.K. Petersen, S.S. Iyengar, T.J.F. Day, G.A. Voth, The hydrated proton at the water liquid/vapor interface, J. Phys. Chem. B 108 (2004) 14804–14806.
- J.G. Li, M. Ikeda, Ch. Tang, Y. Moriyoshi, H. Hamanaka, T. Ishigaki, Chlorinated nanocrystalline TiO₂ powders via one-step Ar/O₂ radio frequency thermal plasma oxidizing mists of TiCl₃ solution: phase structure and photocatalytic performance, J. Phys. Chem. C 111 (2007) 18018–18024.
- I. Siretanu, J.P. Chapel, C. Drummond, Water-ions induced nanostructuration of hydrophobic polymer surfaces, ACS Nano 5 (2011) 2939–2947.
- S. Luchi, H. Chen, S. Paesani, G.A. Voth, Hydrated excess proton at water-hydrophobic interfaces, J. Phys. Chem. B 113 (2009) 4017–4030.
- Y.H. Zhang, C.K. Chan, J.F. Porter, W. Guo, Micro-Raman spectroscopic characterization of nanosized TiO₂ powders prepared by vapor hydrolysis, J. Mater. Res. 13 (1998) 2602–2609.
- J.C. Parker, R.W. Siegel, Calibration of the Raman spectrum to the oxygen stoichiometry of nanophasic TiO₂, Appl. Phys. Lett. 57 (1990) 943–945.
- J.C. Parker, R.W. Siegel, Raman microprobe study of nanophasic TiO₂ and oxidation-induced spectral changes, J. Mater. Res. 5 (1990) 1246–1252.
- G.A. Tompsett, G.A. Bowmaker, R.P. Coony, J.B. Metson, K.A. Rodgers, J.M. Seakins, The Raman spectrum of brookite TiO₂ (Pbca, Z=8), J. Raman Spectrosc. 26 (1995) 57–62.
- Y. Zhu, T. Liu, C. Ding, Structural characterization of TiO₂ ultrafine particles, J. Mater. Res. 14 (1999) 442–446.
- F. Tian, Y. Zhang, J. Zhang, C. Pan, Raman spectroscopy: a new approach to measure the percentage of anatase TiO₂ exposed (001) facets, J. Phys. Chem. C 116 (2012) 7515–7519.
- H. Sun, S. Wang, H.M. Ang, M.O. Tadé, Q. Li, Halogen element modified titanium dioxide for visible light photocatalysis, Chem. Eng. J. 162 (2010) 437–447.
- H. Xu, Z. Zheng, L.Z. Zhang, H.L. Zhang, F. Deng, Hierarchical chlorine-doped rutile TiO₂ spherical clusters of nanorods: large-scale synthesis and high photocatalytic activity, J. Solid State Chem. 181 (2008) 2516–2522.
- J. Kim, U.W. Schmitt, J.A. Gruetzmaier, G.A. Voth, N.E. Scherer, The vibrational spectrum of the hydrated proton: comparison of experiment, simulation, and normal mode analysis, J. Chem. Phys. 116 (2002) 737–746.
- M. Park, I. Shin, N.J. Singh, K.S. Kim, Eigen and Zundel forms of small protonated water clusters: structures and infrared spectra, J. Phys. Chem. A 111 (2007) 10692–10702.
- L.F. Scatena, M.G. Brown, G.L. Richmond, Water at hydrophobic surfaces: weak hydrogen bonding and strong orientation effects, Science 292 (2001) 908–912.
- K. Chhor, J.F. Bocquet, C. Pommier, Syntheses of submicron TiO₂ powders in vapor liquid and supercritical phases, a comparative study, Mater. Chem. Phys. 32 (1992) 249–254.
- T. Bezrodna, G. Puchkovska, V. Shymanovska, J. Baran, H. Ratajczak, IR-analysis of H-bonded H₂O on the pure TiO₂ surface, J. Mol. Struct. 700 (2004) 175–181.
- D.S. Warren, A.J. McQuillan, Influence of adsorbed water on phonon and UV-induced IR absorptions of TiO₂ photocatalytic particle films, J. Phys. Chem. B 108 (2004) 19373–19379.
- R. Nakamura, A. Imanishi, K. Murakoshi, Y. Nakato, In situ FTIR studies of primary intermediates of photocatalytic reactions on nanocrystalline TiO₂ films in contact with aqueous solutions, J. Am. Chem. Soc. 125 (2003) 7443–7450.
- S. Neubert, D. Mitoraj, S.A. Shevlin, P. Pulisova, M. Heimann, Y. Du, G.K.L. Goh, M. Pacia, K. Kruczak, S. Turner, W. Macyk, Z.X. Guo, R.K. Hocking, R. Beranek, Highly efficient rutile TiO₂ photocatalysts with single Cu(II) and Fe(III) surface catalytic sites, J. Mater. Chem. A 4 (2016) 3127–3138.
- D.A. Panayotov, J.T. Yates Jr., Depletion of conduction band electrons in TiO₂ by water chemisorptions – IR spectroscopic studies of the independence of

Ti–OH frequencies on electron concentration, *Chem. Phys. Lett.* 410 (2005) 11–17.

[58] J.B. Kinney, R.H. Staley, Reactions of titanium tetrachloride and trimethylaluminum at silica surfaces studied by using infrared photoacoustic spectroscopy, *J. Phys. Chem.* 87 (1983) 3735–3740.

[59] B.C. Trasferetti, C.U. Davanzo, Berreman effect applied to phase characterization of thin films supported on metallic substrates: the case of TiO_2 , *Phys. Rev. B* 64 (2001) 125404.

[60] J. Soria, J. Sanz, I. Sobrados, J.M. Coronado, M.D. Hernández-Alonso, F.J. Fresno, FTIR and NMR study of the adsorbed water on nanocrystalline anatase, *J. Phys. Chem. C* 111 (2007) 10590–10596.

[61] J. Soria, J. Sanz, I. Sobrados, J.M. Coronado, M.D. Hernández-Alonso, F. Fresno, Water-hydroxyl interactions on small anatase nanoparticles prepared by the hydrothermal route, *J. Phys. Chem. C* 114 (2010) 16534–16540.

[62] A.Y. Nosaka, T. Fujiwara, H. Akutsu, Y. Nosaka, Characteristics of water adsorbed on TiO_2 photocatalytic systems with increasing temperature as studied by solid-state ^1H NMR spectroscopy, *J. Phys. Chem. B* 108 (2004) 9121–9125.

[63] S. Yurdakal, V. Augugliaro, J. Sanz, J. Soria, I. Sobrados, M.J. Torralvo, The influence of the anatase nanoparticles boundaries on the titania activity performance, *J. Catal.* 309 (2014) 97–104.

[64] H.Q. Sun, S.B. Wang, H.M. Ang, M.O. Tade, Q. Li, Halogen element modified titanium dioxide for visible light photocatalysis, *Chem. Eng. J.* 162 (2008) 437–447.

[65] F. Le Normand, J. Barrault, R. Breault, L. Hilaire, A. Kiennemann, Catalysis with palladium deposited on rare earth oxides: influence of the support on reforming and syngas activity and selectivity, *J. Phys. Chem. B* 95 (1991) 257–269.

[66] Y. Lei, B. Liu, J.L. Lu, J.A. Libera, J.P. Greeley, J.W. Elam, Effects of chlorine in titanium oxide on palladium atomic layer deposition, *J. Phys. Chem. C* 118 (2014) 22611–22619.

[67] J. Soria, J. Sanz, I. Sobrados, J.M. Coronado, F. Fresno, M.D. Hernandez Alonso, Magnetic resonance study of the defects influence on the surface characteristics of nanosize anatase, *Cat. Today* 129 (2007) 240–246.